

Quantifying quantum computational complexity via information scrambling

Arash Ahmadi* and Eliska Greplova

Kavli Institute of Nanoscience, Delft University of Technology, Delft, the Netherlands

The advent of quantum technologies brought forward much attention to the theoretical characterization of the computational resources they provide. One outstanding challenge to such characterization is the mathematical complexity that their evaluation possesses. A method to quantify quantum computational complexity is to use a class of functions called magic monotones, which are, however, notoriously hard and impractical to evaluate. In this work, we provide a new perspective on calculating magic monotones by connecting them to the concept of information scrambling. Specifically, we establish a connection between information scrambling in random quantum circuits and the magic these circuits generate. This connection allows us to establish a novel, experimentally scalable way to approximate magic monotones in an arbitrary Hilbert space dimension and therefore evaluate the amount of quantum resources using out-of-time-order correlator measurements. Furthermore, we exploit our result connecting scrambling and magic to formulate a simple criterion to determine chaoticity of a given Hamiltonian.

I. INTRODUCTION

The field of quantum computing introduced the concept that quantum systems can deliver a significant computational speed-up in a variety of settings [1–6]. Yet, although increasingly large quantum processors are available, the question remains of how to rigorously quantify the computational resources of a quantum computer. One successful approach towards determining quantum resources of a quantum state is to calculate how “far away” the state is from being possible to simulate efficiently with a classical computer [7].

A specific example of quantum states that are tractable to represent and simulate on a classical computer are the so-called stabilizer states [8]. These states result from quantum circuits produced by Clifford gates which are elements of the Clifford group generated by the Hadamard gate, the phase gate and the entangling control-NOT gate [9]. The degree to which a given quantum state cannot be approximated by Clifford gates is referred to as magic [10]. The states that are not stabilizer states are called *magic states*. Interestingly, in the context of quantum error correction, the Clifford gates can be implemented fault-tolerantly [11, 12], while universal gates set are achieved by the distillation of a large number of (noisy) magic states into a less-noisy magic state which subsequently provide the computational resources for the fault-tolerant quantum computation [7].

Magic states are generated by quantum gates that are outside of the Clifford group, for example by T-gate, which for qubits corresponds to $\pi/4$ -rotation around the Z -axis. The degree of non-Cliffordness generated depends on where in a quantum circuit the T-gate was applied, e.g. a T-gate applied to the $|0\rangle$ -state leaves the state unaltered and no magic is produced. Non-Cliffordness is quantified in this sense using magic monotones that assign a numerical value to how far a given

state is from being Clifford. Examples of magic monotones include magical cross-entropy, mana [10], and robustness of magic [13]. These measures are, however, computationally expensive to evaluate and their calculation requires exact knowledge of the wave-function combined with complex optimization [10], which excludes the study of large quantum circuits.

Another approach to describe how quantum a specific state is, relates to the amount of quantum correlations in the system via various entanglement measures [14]. A simple consideration shows that while there might be a relation between entanglement and magic they are not identical. For instance, a maximally entangled state of two qubits can be achieved by a Clifford circuit and, thus, contains no magic. On the other hand, the states that are generated complex non-Clifford circuits do generally exhibit complex many-body entanglement [15]. A related concept is that of information scrambling [16]. Through the time evolution of a closed quantum system, the information about initial state of the system can become very hard to access due to quantum correlations in the system [17]. Even though the information is still encoded in the system it is not accessible without measuring all its degrees of freedom. Information scrambling has recently attracted an increasing amount of attention due to the relation with the anti-de Sitter/conformal field theory (AdS/CFT) correspondence [18]. The AdS/CFT correspondence draws a duality that relates the noise in quantum error correction codes to information scrambling in black holes [19–21]. Another applications of this concept emerged in condensed matter physics such as many-body localization [22] and non-Fermi liquid behaviors [23].

Moreover, it was recently experimentally demonstrated [24] that out-of-time-correlators (OTOC) used to characterize the degree of information scrambling in a quantum system [16, 19–21, 25, 26] can be used to determine the degree of non-Cliffordness of scrambling quantum circuits. The separate progress in characterizing quantum complexity in terms of both non-Cliffordness and correlation-induced information scrambling raises an interesting question of whether and how the two concepts

* a.ahmadi-1@tudelft.nl

are related.

In this work we formalize the relation between entanglement and non-Cliffordness based characterizations of quantum computational complexity. Specifically we show that there exists a direct fundamental relation between fluctuations in out-of-time-order correlators of a quantum circuit and the average magic these circuits generate. Capitalizing on this relation, we put forward an experimentally feasible way to approximating mana using the evaluation of OTOC. The OTOC evaluation is accessible for high number of qubits using modern computational techniques like tensor networks [27] and neural networks [28]. Moreover, OTOC measurements are also experimentally accessible [24]. The unique aspect of our approach is related to the measurement scaling and the experimental feasibility. It has been shown that there exist an analytical relation between entanglement and non-Cliffordness [29]. In practice this requires measuring the entanglement and the exponential scaling of the Hilbert space dimension results in challenges for larger system sizes. The approach presented here is relying on the measurement of OTOCs which has been shown to be readily accessible for tens of qubits with a small number of measurements [24].

II. MAGIC

The concept of magic in quantum information science arises from the field of resource theory [30]. The Gottesman-Knill theorem [8] guarantees that the subset of the physical states known as *stabilizer* states are efficiently simulatable on a classical computer. More precisely, the stabilizer states are the second level of the Clifford hierarchy [9].

Since the first level (the Pauli gates) and the second level (the Clifford gates) of the Clifford hierarchy are insufficient for universal quantum computing, we need to use the third level gates. This level of Clifford hierarchy includes the above-mentioned T-gate. Another set of important non-Clifford gates are the rotation gates $\{R_x(\theta), R_y(\theta), R_z(\theta)\}$, where θ is the angle of rotation. These gates are particularly important in problems that require a continuous set of parameters to tune, i.e. quantum machine learning algorithms [5, 6].

The amount of non-Cliffordness, or magic, of any state is measured using *magic monotones*. Magic monotones such as robustness of magic are based on an optimization over all stabilizer states, which make them practically hard to compute. However, one example of a magic monotone that does not require any optimization is known as mana, \mathcal{M} [10]. This magic monotone has another limitation namely that it is only definable for odd-prime dimensional Hilbert spaces. Also, mana is practically very hard to calculate since it is based on calculating discrete Wigner function which in practice limits calculations to at most 7 qudits. More details regarding the definition and evaluation of mana are available in

Appendix A.

III. INFORMATION SCRAMBLING

A well-known measure of information scrambling is the out-of-time-order correlators (OTOC) which is commonly used in high-energy physics and condensed matter physics [16, 19–23, 25, 26]. OTOC is evaluated for any two operators W and V as

$$OTOC(t) = \text{Re}(\langle W^\dagger(t)V^\dagger W(t)V \rangle), \quad (1)$$

where

$$W(t) = U^\dagger(t)W(0)U(t), \quad (2)$$

and $U(t)$ is the time evolution operator, which could either result from time evolution of a Hamiltonian or from a quantum circuit. Here we will consider a N qudit system and we take $W(0) = X_{N-1}$ and $V = Z_1$ where X_i and Z_i are the conventional Pauli gates and the subscript is the i -th qudit. In this case, $W(0)$ plays the role of the Butterfly operator in studying chaotic quantum systems. The reason for using butterfly operator is that by including a small perturbation (in this case a bit flip) we are disturbing the reversibility of the system, which is a signature of chaos [31]. The information scrambling measured through OTOC describes how information spreads in the system and becomes inaccessible in later times [16, 19–21, 25, 26]. It also describes how local Heisenberg operators grow in time [24, 32, 33]. A way to assess how the OTOC value fluctuates over a set of random circuits is the OTOC fluctuation, δ_{OTOC} , defined as the standard deviation of OTOC over all instances.

IV. EXPRESSING MAGIC MONOTONES AS SCRAMBLING CORRELATORS

We will now investigate the relation between the fluctuations of OTOC, which was experimentally observed in Ref. [24] to decrease with the growing non-Cliffordness of the quantum circuit, and the measure for quantum complexity, mana, \mathcal{M} . To this end, we design random quantum circuits with Clifford and non-Clifford gates. First, we consider N qudits in q -dimensional Hilbert space where $q \in \{2, 3, 5\}$. The circuits consist of M cycles of gates. In each cycle, we first apply one single Clifford gate from the set $\mathcal{S} = \{H, S, X, Z, I\}$ on each qudit such that each element has 20% probability to be applied per qudit. Then we add two *Sum* gates on two randomly chosen qudits, where the *Sum* gate is the counterpart of CNOT in Hilbert spaces with $q > 2$. Finally, we follow these Clifford gates by adding a single non-Clifford gate, $R_z(\theta^q)$, with varying probability, \mathcal{P} , such that the quantum complexity of the circuit is correspondingly varied. The parameter θ^q , which is increasing monotonically from zero to θ_{max}^q , is tuning the amount

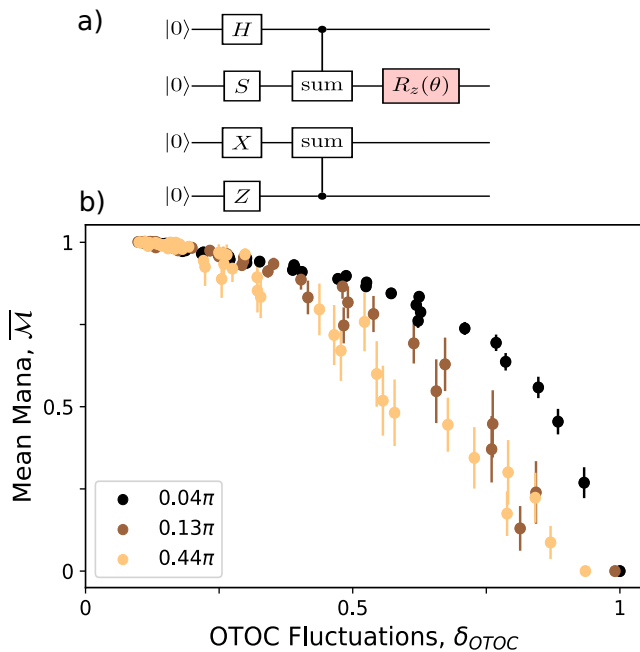


Figure 1. (a) An example of a cycle of a random circuit. In the beginning of each cycle, we apply single-qutrit Clifford gates. Two entangling gates follow in the next step and, finally, with probability \mathcal{P} we add the non-Clifford gate $R_z(\theta)$. (b) The mean mana, $\overline{\mathcal{M}}$ vs. the fluctuations of OTOC, δ_{OTOC} for 4 qutrits for three different values of θ^3 of the rotation gate. The number of instances for all cases is 50, and the depth of the circuits are 200 for $\theta^3 = 0.04\pi$, 60 for $\theta^3 = 0.13\pi$ and 25 for $\theta^3 = 0.44\pi$. The error bar on the plot corresponds to standard deviation of mana, \mathcal{M} over all instances in each step.

of non-Cliffordness added into the circuit. The value of the angle θ_{max}^q is dependent on the local Hilbert space dimension, q , and we will elaborate on its precise values below. We show the scheme of the basic building block, or one cycle, of the circuit in Fig. 1(a).

We begin by analyzing the relationship of mana and OTOC in the Hilbert space of dimension $q = 3$ for circuits containing four qutrits such that mana is well defined and computationally tractable. We use the qutrit Clifford gates introduced in [34] and we use the generalized X -operator as a butterfly operator. We provide detailed definitions of all gates in Appendix B.

We observe a decreasing monotonous relation between the mean value of mana, $\overline{\mathcal{M}}$ and the OTOC fluctuations, δ_{OTOC} , see Fig. 1(b). Here $\overline{\mathcal{M}}$ and δ_{OTOC} was evaluated for three non-Clifford rotation angles $\theta^3 \in \{0.04\pi, 0.13\pi, 0.44\pi\}$ over $K = 50$ instances per acceptance probability of non-Clifford gate value, \mathcal{P} . In total we consider 50 discrete steps in $\mathcal{P} \in [0, 1]$. Note that mana is an extensive function [35], so we normalize it with respect to local Hilbert space dimension, q and number of qutrits, N . This normalization is performed for ease of comparison between different Hilbert space dimensions. Additionally, we observe that the angle of the

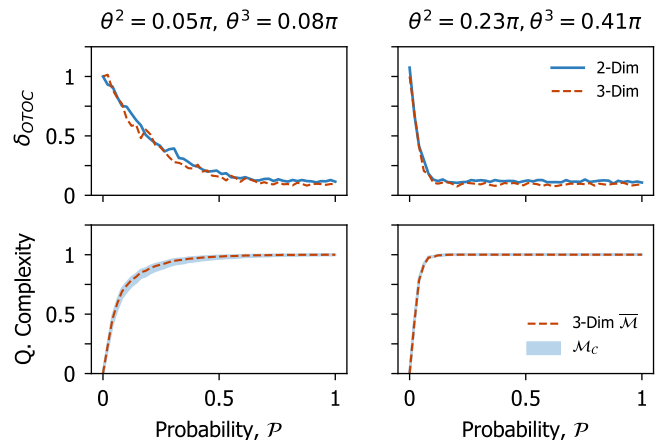


Figure 2. *The upper panels:* The OTOC fluctuations, δ_{OTOC} over 50 instances as a function of the acceptance probability, \mathcal{P} of non-Clifford gate, $R_z(\theta^2)$, in each cycle. The solid lines are the values of δ_{OTOC}^2 and the dashed lines are the corresponding δ_{OTOC}^3 with the highest correlations. *The lower panels:* The Quantum Complexity over 50 instances as a function of probability of acceptance of non-Clifford gate, $R_z(\theta^2)$, in each cycle. The light blue areas correspond to the correlator mana, \mathcal{M}_c of the circuit of qubits resulted from $corr(\delta_{OTOC}^3, \delta_{OTOC}^2)$ along side the exact values of $\overline{\mathcal{M}}^3$ (red line). We have used 4 qutrits for both 2 and 3 dimensional Hilbert spaces.

non-Clifford gate influences the curvature of this relation between $\overline{\mathcal{M}}$ and δ_{OTOC} . The smallest $\theta^3 = 0.04\pi$ corresponds to the least non-Cliffordness injected into the circuit, while the largest one $\theta^3 = 0.44\pi \approx \frac{4\pi}{9}$ corresponds to the T-gate limit for qutrits, and therefore to maximum non-Cliffordness in our setting. We simulated the angles $\theta^3 \in \{0.04\pi, 0.13\pi, 0.44\pi\}$ with circuit depths $M \in \{200, 60, 25\}$ cycles, respectively. For the simulation of the quantum circuits we have used the Cirq package [36].

In summary, this numerical experiment shows that sampling out-of-time-order correlators of random circuits allows us to estimate the non-Cliffordness, or magic, produced by the set of random circuits with the fixed probability \mathcal{P} . Notably, the amount of measurements one needs to perform to make this estimation is very low. Specifically, measuring OTOC is experimentally very accessible since it requires merely a single qutrit measurements on one of the qutrits in the output layer of the quantum circuit [24].

V. CORRELATOR MANA

Having a straightforward way to estimate the average amount of magic generated by a class of quantum circuits from a small amount of measurements is a stepping stone towards defining a quantity that can be constructed from OTOC fluctuations, δ_{OTOC} , and approximate mana ef-

ficiently. Moreover, note that the numerical calculation or experimental measurement of OTOC fluctuations are, in difference from mana, not restricted by local Hilbert space dimension. Here, we define this approximating quantity as *correlator mana*, \mathcal{M}_C and we show how to construct it for quantum circuits of qudits with arbitrary local Hilbert space dimension.

Specifically, we propose the following algorithm to evaluate correlator mana: We consider two quantum circuits with qudits with local dimension q and w respectively. For both of these circuits we can sample δ_{OTOC} as a function of non-Clifford gate parameter θ^q and θ^w respectively. By minimizing the Pearson correlation [37] of $corr(\delta_{OTOC}^q, \delta_{OTOC}^w)$, we find the values of θ^q and θ^w for which the difference between δ_{OTOC}^q and δ_{OTOC}^w is minimal. Since, for numerical reasons, both θ^q and θ^w are discretized, we are unlikely to find correlation $corr = 1$. For this reason we consider δ_{OTOC}^q and δ_{OTOC}^w to be fully correlated for $corr \geq 0.98$. The details of Pearson correlation calculation can be found in Appendix D.

To demonstrate the utility of our result, consider the example of calculating correlator mana for qubits ($q = 2$) using the knowledge of how to calculate mana for qutrits ($w = 3$). We calculate OTOC fluctuations for qubits, δ_{OTOC}^2 for a circuit parametrized by a specific angle θ_s^2 that we are interested in. We follow by evaluation of qutrit OTOC fluctuations, δ_{OTOC}^3 for a set of angles $\theta^3 \in (0, 4\pi/9)$ to find the angle θ_{opt}^3 for which the correlation $corr(\delta_{OTOC}^3, \delta_{OTOC}^2)$ is maximal. We then conclude that $\overline{\mathcal{M}}$ generated by the qutrit circuit with θ_{opt}^3 is the same as the correlator mana \mathcal{M}_C of the sought-after qubit circuit parametrized by θ_s^2 . We show results of this procedure in Fig. 2, where the top two panels show the optimized OTOC fluctuations for two example values of $\theta_s^2 \in \{0.05\pi, 0.23\pi\}$. The bottom panels show the corresponding $\overline{\mathcal{M}}$ and correlator mana. Note that correlator mana value has a uncertainty caused by the discretization discussed above.

To verify the reliability of the mana extrapolation method explained above, we repeat the algorithm for $q = 3, w = 5$, i.e. two odd-dimensional Hilbert spaces, where $\overline{\mathcal{M}}$ can be calculated exactly. We then proceed to calculate correlator mana for the qutrit circuit assuming we only have access to $\overline{\mathcal{M}}$ of five-dimensional qudit circuit. We find the correlator mana for qutrits from maximizing $corr(\delta_{OTOC}^5, \delta_{OTOC}^3)$ where $\theta^5 \in (0, \frac{\pi}{2})$ for two different values of $\theta_s^3 \in \{0.05\pi, 0.4\pi\}$ and, in Fig. 3, we see that the exact values of mana for each of θ_s^3 fit in the region of the correlator mana with perfect agreement.

VI. CHAOS

One of the key results in the field of information scrambling is the precise formulation of relation between chaos and out-of-time-order correlators. Specifically, chaotic systems manifest the exponential behaviour of OTOC values [16, 21, 38, 39]. A standard way to characterize

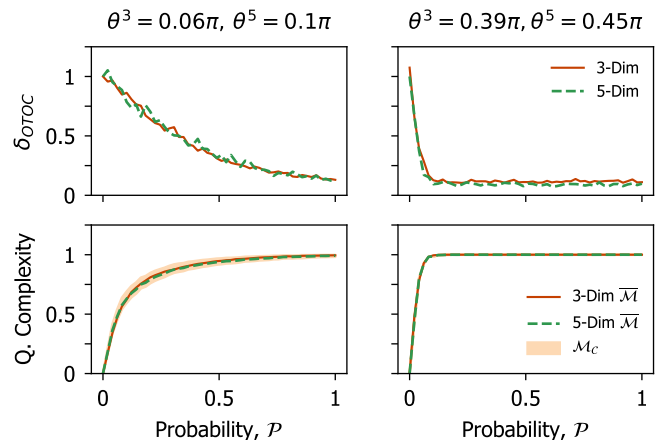


Figure 3. *The upper panels:* The δ_{OTOC} over 50 instances as a function of probability of acceptance of non-Clifford gate, $R_z(\theta^3)$, in each cycle. The solid lines are the values of δ_{OTOC}^3 and the dashed lines are the corresponding δ_{OTOC}^5 with the highest correlations. *The lower panels:* The Quantum Complexity over 50 instances as a function of probability of acceptance of non-Clifford gate, $R_z(\theta^3)$, in each cycle. The light orange area are the correlator Mana of the circuit of qutrits resulted from $corr(\delta_{OTOC}^5, \delta_{OTOC}^3)$ along side the exact values of $\overline{\mathcal{M}}^3$ (red line) and $\overline{\mathcal{M}}^5$ (dashed green line). We have used 4 qudits for 3 dimensional Hilbert space and 3 qudits for 5 dimensional Hilbert space.

the degree of chaos of quantum many-body systems is to consider a distribution of differences between consecutive eigenenergies of the Hamiltonian. If this distribution is Poissonian, the system is non-chaotic. The systems that are, on the other hand, strongly chaotic have distributions that follow a Wigner-Dyson distribution [40–42].

Analogously, in Ref. [43] it was shown that the magic monotone of a time-evolved state under chaotic systems saturates, while for non-chaotic time evolved states the magic monotone shows a periodic behaviour. While this is a profound connection, the question of practically accessing the mana of a system remains. Here, we reformulate these statements in the language of the easy-to-access OTOC fluctuations.

The protocol that we introduce is the following as also illustrated in Fig. 4(a): *Step 1:* We prepare the initial state in the computational basis $|0\rangle^{\otimes N}$. *Step 2:* We apply the time evolution of the desired Hamiltonian, $U_H(t)$. *Step 3:* We follow the time-evolution with the application of a random Clifford unitary circuit, U_C with a sufficient depth to get fully scrambled. Here we have used a depth of 50 cycles with $\mathcal{P} = 0$. *Step 4:* We repeat the whole process for $K = 50$ number of instances.

The chosen design of the quantum circuit enable us to clearly distinguish between chaotic and non-chaotic regime. We observed that for non-chaotic Hamiltonians, $\delta_{OTOC} = 0$ for all times, t . For chaotic Hamiltonians, on the other hand, $\delta_{OTOC} \rightarrow 0$ as the number of qubits

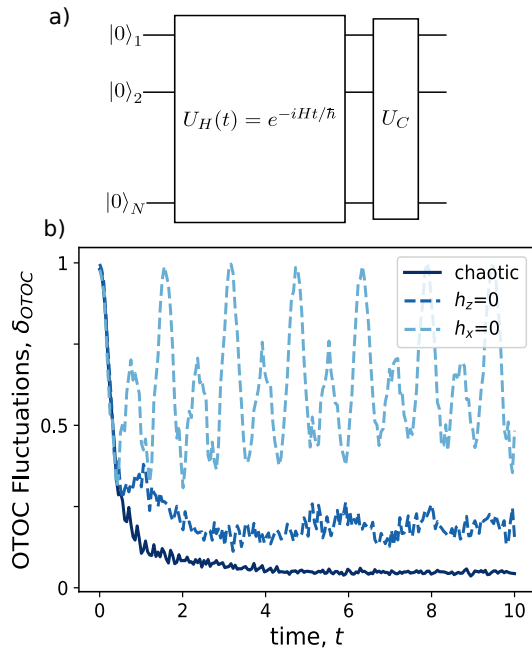


Figure 4. (a) The schematic circuit for determining the chaoticity of the Hamiltonian H . (b) δ_{OTOC} for 8 qubits under time evolution of Ising spin chain in strongly chaotic regime $(h_x, h_z) = (-1.05, 0.5)$ (dark blue solid line) and in two examples of non-chaotic regime (dashed lines), followed by a random Clifford circuit of depth 50. We have used 8 qubits for this simulation.

increases [44]. This fact would then complicate defining a clear-cut distinction between chaotic and non-chaotic regimes especially in for the large N systems. By adding the Clifford block, U_C , we force the initial point of OTOC fluctuations at the time $t = 0$ to be $\delta_{OTOC} = 1$. After engineering this initial condition we can observe the dependence of the OTOC fluctuations on the degree of chaos of the Hamiltonian, see Fig. 4(b).

To exemplify our protocol, we choose an Ising spin chain with open boundary conditions with longitudinal (h_z) and transverse (h_x) magnetic fields

$$H = \sum_n -S_z^n S_z^{n+1} - h_x S_x^n - h_z S_z^n \quad (3)$$

It is well-known that when h_x or h_z vanish, the Hamiltonian of Eq.(3) is non-chaotic and it is strongly chaotic if $(h_x, h_z) = (-1.05, 0.5)$ [39]. By calculating the OTOC fluctuations, δ_{OTOC} with the proposed protocol we can see that chaoticity is easily distinguishable for Ising spin chain in Fig. 4(b). We have used the Qiskit package [45] to produce the time evolution of the Hamiltonian of Eq.(3), $U_H(t)$. This method overcomes the challenge of calculating magic monotone to determine chaoticity or access to the whole energy spectrum to determine the nearest-neighbor eigenenergy spacing distribution. As we expect, the universal random circuits that we have been using so far are chaotic and we have seen the saturation

of δ_{OTOC} in Fig. 2 and Fig. 3. We also calculated correlator mana, \mathcal{M}_C for the Ising spin chain in chaotic regime in the Appendix C.

VII. CONCLUSION AND DISCUSSION

We have shown that there exists a robust monotonous relationship between information scrambling and magic monotones. Specifically, we observed that average non-Cliffordness produced by a set of random circuits with the same hyper-parameters is on average inversely proportional to out-of-time-order correlator fluctuations over that same set of circuits. Theoretically, this result constitutes an addition to recent discoveries hinting at a deep relationship between magic and various entanglement characterization of quantum states. Practically, we provide evidence that a small set of easily experimentally accessible OTOCs contains the same information about non-Cliffordness generated by a quantum circuit as magic monotones of the output state would.

Additionally, the relationship between OTOCs and mana allowed us to define a mana approximator, the so-called correlator mana, for quantum circuits with even local dimension e.g. for qubits.

Recent related work have shown that the Renyi entropy can be regarded as magic measure [46] and can be calculated and measured experimentally for qubits as well [47–50] although the number of measurements increases exponentially with the number of qubits and amount of non-Cliffordness of the states. Equivalently, the relation of the Renyi entropy and OTOC has been established, and another similar relation for magic monotones has been shown [29], which still requires an exponential increase of the number of measurements with the Hilbert space size. Additional magic monotone was recently proposed relying on Bell measurement [51].

The method we are proposing here is based on the statistical behaviour of OTOC and only a small number of measurements is sufficient for tens of qubits, which makes it readily available both numerically and experimentally [24]. More specifically OTOC can be evaluated numerically for up to 20 qubits with conventional methods and it is also calculable beyond this using modern methods like tensor networks [27] and neural networks [28]. Finally, using the knowledge of saturation of magic in chaotic systems and oscillatory behaviour in non-chaotic regimes [43], we proposed a protocol to determine the chaoticity of a quantum system with finite amount of measurements. We expect that the relation between computational power and readily measurable correlation functions presented in this work can shed new light on the abilities provided by large-scale quantum computers.

All code required to reproduce results presented in this manuscript is available at [52].

Appendix A: The calculable magic monotone: mana

One of the magic monotones is known as *mana*. The restriction of mana is that it is only well-defined for odd prime dimensional Hilbert spaces. Here, we introduce it for q -dim Hilbert spaces [10] with q an odd prime number. To show how to calculate mana, we first need to define the clock and shift operators corresponding to the q -dimensional Pauli Z gate and Pauli X gate [34],

$$Z = \sum_{n=0}^{q-1} \omega^n |n\rangle \langle n|, \quad X = \sum_{n=0}^{q-1} |n+1 \bmod q\rangle \langle n| \quad (\text{A1})$$

with $\omega = e^{2\pi i/q}$. The other necessary definition is the Heisenberg-Weyl operators in prime dimensions,

$$T_{aa'} = \omega^{-2^{-1}aa'} Z^a X^{a'} \quad (\text{A2})$$

where $2^{-1} = \frac{q+1}{2}$ (the multiplicative inverse of 2 mod q) and $(a, a') \in \mathbb{Z}_q \times \mathbb{Z}_q$. By following this definition, we can define Pauli strings as

$$T_{\mathbf{a}} = T_{a_1 a'_1} \otimes T_{a_2 a'_2} \dots \otimes T_{a_N a'_N}. \quad (\text{A3})$$

Now, we can define new basis set for the Hilbert space know as **phase space point operators**,

$$A_{\mathbf{b}} = q^{-N} T_{\mathbf{b}} [\sum_{\mathbf{a}} T_{\mathbf{a}}] T_{\mathbf{b}}^\dagger \quad (\text{A4})$$

and these phase space point operators form a complete basis set for $\mathbb{C}^{q^N \otimes q^N}$. Thus, we can expand any density matrix ρ in this basis,

$$\rho = \sum_{\mathbf{u}} W_\rho(\mathbf{u}) A_{\mathbf{u}} \quad (\text{A5})$$

The coefficients $W_\rho(\mathbf{u})$ are called discrete Wigner functions and we can define mana as

$$\mathcal{M}(\rho) = \frac{1}{N} \log \sum_{\mathbf{u}} |W_\rho(\mathbf{u})| \quad (\text{A6})$$

As we already stated in the main text, we are dealing with Clifford and non-Clifford operations. The Clifford gates map Pauli strings to other Pauli strings, up to an arbitrary phase [35],

$$C = \{U : UT_{\mathbf{a}}U^\dagger = e^{i\phi} T_{\mathbf{b}}\}. \quad (\text{A7})$$

Since the Clifford gates map each of these Pauli strings to each other, each Clifford unitaries also map the computational basis to one of the eigenstates of Pauli strings. These eigenstates are called **stabilizer states**. Since stabilizer states are prepared with only Clifford gates, their mana is *zero*.

Appendix B: Clifford and non-Clifford gates definitions

In this appendix we are introducing the gates that we have used in this study. We introduce both for 2-dimensional Hilbert spaces and higher dimensional Hilbert spaces.

1. Clifford gates

The set of Clifford gates is the second level of Clifford hierarchy [9] that are the following gates in 2-dimensional Hilbert spaces,

$$H_2 = \frac{1}{\sqrt{2}} \begin{bmatrix} 1 & 1 \\ 1 & -1 \end{bmatrix}, \quad P_2 = \begin{bmatrix} 1 & 0 \\ 0 & i \end{bmatrix} \quad (\text{B1})$$

$$\text{CNOT} = |0\rangle \langle 0| \otimes I + |1\rangle \langle 1| \otimes X$$

The generalization of these gates is straightforward [53]. The d -dimensional Hadamard gate, H_d , is

$$H_d |j\rangle = \frac{1}{\sqrt{d}} \sum_{i=0}^{d-1} \omega^{ij} |i\rangle \quad j \in \{0, 1, 2, \dots, d-1\} \quad (\text{B2})$$

where $\omega := e^{2\pi i/d}$. The next gate is the d -dimensional Phase gate, P_d ,

$$P_d |j\rangle = \omega^{j(j-1)/2} |j\rangle \quad (\text{B3})$$

and, finally, the generalized CNOT gate that is known as SUM_d gate and defined as

$$SUM_d |i, j\rangle = |i, i+j \pmod{d}\rangle \quad i, j \in \{0, 1, 2, \dots, d-1\} \quad (\text{B4})$$

2. Non-Clifford gates

Clifford gates are not sufficient for universal quantum computation and we at least need one non-Clifford gate to have this universality [54, 55]. One of these gate is the T-gate that emerges from the third level Clifford hierarchy. The definition of T-gate for 2-dimensional Hilbert space is

$$T_2 = \begin{bmatrix} 1 & 0 \\ 0 & e^{i\pi/4} \end{bmatrix} \quad (\text{B5})$$

The generalization of T-gate to higher dimensional Hilbert spaces is not so straightforward [34]. Here, we only write down the matrices of the T-gate for 3-dimensional and 5-dimensional Hilbert spaces which are useful for us. The 3-dimensional Hilbert space T-gate is

$$T_3 = \begin{bmatrix} 1 & 0 & 0 \\ 0 & e^{2\pi i/9} & 0 \\ 0 & 0 & e^{-2\pi i/9} \end{bmatrix}, \quad (\text{B6})$$

Additionally, the T-gate of a 5-dimensional Hilbert space is

$$T_5 = \begin{bmatrix} 1 & 0 & 0 & 0 & 0 \\ 0 & e^{-4\pi i/5} & 0 & 0 & 0 \\ 0 & 0 & e^{-2\pi i/5} & 0 & 0 \\ 0 & 0 & 0 & e^{4\pi i/5} & 0 \\ 0 & 0 & 0 & 0 & e^{2\pi i/5} \end{bmatrix} \quad (\text{B7})$$

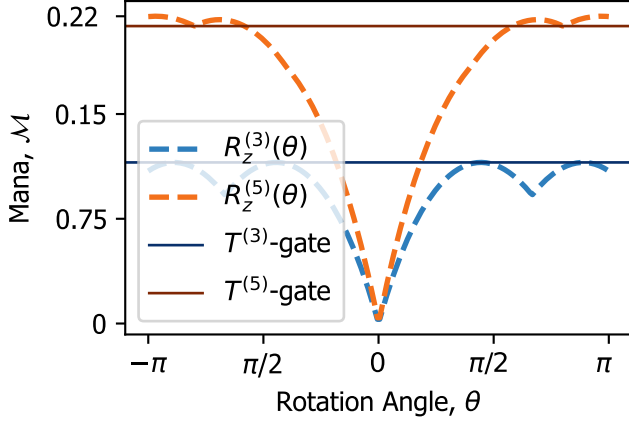


Figure 5. The value of mana of a random circuit with only one non-Clifford gate in it. The circuit consists of 10 layers of the random Clifford cycles of Fig. 1(a), one non-Clifford gate and again 10 layers of the random Clifford cycles. The rotation angle of the non-Clifford varies from $-\pi$ and π . Additionally, with horizontal lines are the mana for the corresponding T-gate for both 3-dimensional and 5-dimensional Hilbert spaces.

Another useful set of non-Clifford gates is using rotation gates. As it is apparent from the T_2 -gate definition, it is $R_z(\pi/4)$ up to some constant phase. So we use

$$R_z^{(2)}(\theta) = e^{-i\theta Z/2} \quad (\text{B8})$$

where Z is the Pauli Z matrix. We have a continuous parameter θ and vary it in $(0, \pi/4)$. In the same procedure, we can see that

$$R_z^{(3)}(\theta) = e^{-i\theta s_z^{12}/2}, \quad s_z^{12} = \begin{bmatrix} 0 & 0 & 0 \\ 0 & 1 & 0 \\ 0 & 0 & -1 \end{bmatrix} \quad (\text{B9})$$

where s_z^{12} is the rotation generator in the 12 subspace. Again we have continuous parameter θ and vary it between $(0, 4\pi/9)$. For 2 and 3-dimensional Hilbert spaces we know that the T-gate is a rotation gate with specific angle but this is not the same situation with 5-dimensional Hilbert space. We considered the rotation gate in 01 subspace,

$$R_z^{(5)}(\theta) = e^{-i\theta s_z^{01}/2}, \quad s_z^{01} = \begin{bmatrix} 1 & 0 & 0 & 0 & 0 \\ 0 & -1 & 0 & 0 & 0 \\ 0 & 0 & 0 & 0 & 0 \\ 0 & 0 & 0 & 0 & 0 \\ 0 & 0 & 0 & 0 & 0 \end{bmatrix} \quad (\text{B10})$$

where s_z^{01} is the rotation generator in the 01 subspace. Since T_5 -gate is not reproducible from a single rotation operator, at least not with Gell-Mann matrices of 5-dimensional Hilbert spaces. While T_5 -gate is not the extreme case of the rotation in 01 subspace, this rotation provides more mana than the T_5 -gate beyond a certain rotation angle, see Fig. 5.

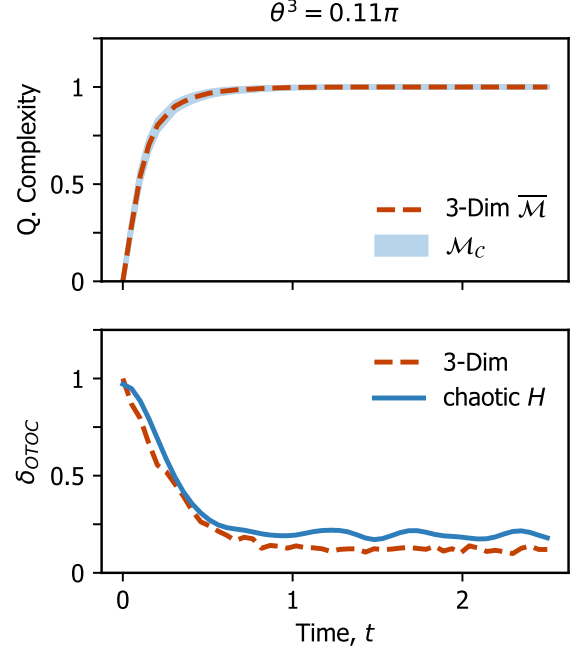


Figure 6. Approximating the correlator mana, \mathcal{M}_C for the strongly chaotic Ising chain of 4 particles.

Appendix C: Correlator mana for chaotic systems

As we observed in the main text, the universal random circuits are also chaotic since magic saturates in those systems. On the other hand, we already introduced a chaotic system in Eq. (3) and we have seen that the fluctuations of OTOC, δ_{OTOC} also saturates for the strongly chaotic regime. A natural extension for the results we introduced in the main text would be calculating correlator mana, \mathcal{M}_C for the system of Eq. (3). Using the method to estimate correlator mana in the main text, we have approximated the correlator mana for the Ising Hamiltonian in Fig. 6.

Appendix D: Pearson correlation

In the section V, in order to find the minimum difference between δ_{OTOC}^q and δ_{OTOC}^w to find the values of θ^q and θ^w that have high similarity of the quantum complexity, we used Pearson correlation. The Pearson correlation [37] is defined as Eq. (D1)

$$corr = \frac{\sum(\delta_{OTOC,i}^q - \overline{\delta_{OTOC}^q})(\delta_{OTOC,i}^w - \overline{\delta_{OTOC}^w})}{\sqrt{\sum(\delta_{OTOC,i}^q - \overline{\delta_{OTOC}^q})^2 \sum(\delta_{OTOC,i}^w - \overline{\delta_{OTOC}^w})^2}} \quad (\text{D1})$$

where the index i stands for the calculated δ_{OTOC} for each acceptance probability \mathcal{P} , as a function of θ . We used the built-in function in the Scipy package to calculate Pearson correlation.

- [1] Peter W. Shor. Polynomial-time algorithms for prime factorization and discrete logarithms on a quantum computer. *SIAM Review*, 41(2):303–332, 1999.
- [2] Lov K. Grover. A fast quantum mechanical algorithm for database search, 1996.
- [3] Scott Aaronson and Alex Arkhipov. The computational complexity of linear optics. *Theory of Computing*, 9(4):143–252, 2013.
- [4] Yudong Cao, Jonathan Romero, Jonathan P. Olson, Matthias Degroote, Peter D. Johnson, Mária Kieferová, Ian D. Kivlichan, Tim Menke, Borja Peropadre, Nicolas P. D. Sawaya, Sukin Sim, Libor Veis, and Alán Aspuru-Guzik. Quantum chemistry in the age of quantum computing. *Chemical Reviews*, 119(19):10856–10915, 2019. PMID: 31469277.
- [5] Abhinav Kandala, Antonio Mezzacapo, Kristan Temme, Maika Takita, Markus Brink, Jerry M. Chow, and Jay M. Gambetta. Hardware-efficient variational quantum eigensolver for small molecules and quantum magnets. *Nature*, 549(7671):242–246, Sep 2017.
- [6] Edward Farhi, Jeffrey Goldstone, and Sam Gutmann. A quantum approximate optimization algorithm, 2014.
- [7] Sergey Bravyi and Alexei Kitaev. Universal quantum computation with ideal clifford gates and noisy ancillas. *Phys. Rev. A*, 71:022316, Feb 2005.
- [8] Daniel Gottesman. The heisenberg representation of quantum computers. 1998.
- [9] Daniel Gottesman and Isaac L. Chuang. Demonstrating the viability of universal quantum computation using teleportation and single-qubit operations. *Nature*, 402(6760):390–393, 1999.
- [10] Victor Veitch, S A Hamed Mousavian, Daniel Gottesman, and Joseph Emerson. The resource theory of stabilizer quantum computation. *New Journal of Physics*, 16(1):013009, 2014.
- [11] Daniel Gottesman. Theory of fault-tolerant quantum computation. *Physical Review A*, 57(1):127–137, jan 1998.
- [12] Peter W. Shor. Fault-tolerant quantum computation, 1996.
- [13] Mark Howard and Earl Campbell. Application of a resource theory for magic states to fault-tolerant quantum computing. *Physical Review Letters*, 118(9), mar 2017.
- [14] Ryszard Horodecki, Paweł Horodecki, Michał Horodecki, and Karol Horodecki. Quantum entanglement. *Reviews of Modern Physics*, 81(2):865–942, jun 2009.
- [15] Sarah True and Alioscia Hama. Transitions in entanglement complexity in random circuits, 2022.
- [16] Pavan Hosur, Xiao-Liang Qi, Daniel A. Roberts, and Beni Yoshida. Chaos in quantum channels. *Journal of High Energy Physics*, 2016(2), Feb 2016.
- [17] Yongliang Zhang. Information scrambling in quantum many-body systems. *Dissertation (Ph.D.)*, Feb 2020.
- [18] Ahmed Almheiri, Xi Dong, and Daniel Harlow. Bulk locality and quantum error correction in ads/cft. *Journal of High Energy Physics*, 2015(4), 2015.
- [19] Stephen H. Shenker and Douglas Stanford. Black holes and the butterfly effect. *Journal of High Energy Physics*, 2014(3):67, March 2014.
- [20] Patrick Hayden and John Preskill. Black holes as mirrors: quantum information in random subsystems. *Journal of High Energy Physics*, 2007(09):120–120, Sep 2007.
- [21] Juan Maldacena, Stephen H. Shenker, and Douglas Stanford. A bound on chaos. *Journal of High Energy Physics*, 2016(8), Aug 2016.
- [22] D.M. Basko, I.L. Aleiner, and B.L. Altshuler. Metal-insulator transition in a weakly interacting many-electron system with localized single-particle states. *Annals of Physics*, 321(5):1126–1205, May 2006.
- [23] Daniel Ben-Zion and John McGreevy. Strange metal from local quantum chaos. *Physical Review B*, 97(15), Apr 2018.
- [24] Xiao Mi, Pedram Roushan, Chris Quintana, Salvatore Mandrà, Jeffrey Marshall, Charles Neill, Frank Arute, Kunal Arya, Juan Atalaya, Ryan Babbush, and et al. Information scrambling in quantum circuits. *Science*, 374(6574):1479–1483, Dec 2021.
- [25] Yasuhiro Sekino and L Susskind. Fast scramblers. *Journal of High Energy Physics*, 2008(10):065–065, oct 2008.
- [26] Daniel A. Roberts and Beni Yoshida. Chaos and complexity by design. *Journal of High Energy Physics*, 2017(4), apr 2017.
- [27] Shenglong Xu and Brian Swingle. Scrambling dynamics and out-of-time ordered correlators in quantum many-body systems: a tutorial, 2022.
- [28] Yukai Wu, L.-M. Duan, and Dong-Ling Deng. Artificial neural network based computation for out-of-time-ordered correlators. *Physical Review B*, 101(21), jun 2020.
- [29] Lorenzo Leone, Salvatore F. E. Oliviero, and Alioscia Hama. Magic hinders quantum certification, 2022.
- [30] Eric Chitambar and Gilad Gour. Quantum resource theories. *Reviews of Modern Physics*, 91(2), Apr 2019.
- [31] Xiao Chen, Rahul M. Nandkishore, and Andrew Lucas. Quantum butterfly effect in polarized floquet systems. *Physical Review B*, 101(6), feb 2020.
- [32] Xiao-Liang Qi and Alexandre Streicher. Quantum epidemiology: operator growth, thermal effects, and SYK. *Journal of High Energy Physics*, 2019(8), aug 2019.
- [33] Daniel E. Parker, Xiangyu Cao, Alexander Avdoshkin, Thomas Scaffidi, and Ehud Altman. A universal operator growth hypothesis. *Physical Review X*, 9(4), oct 2019.
- [34] Yuchen Wang, Zixuan Hu, Barry C. Sanders, and Sabre Kais. Qudits and high-dimensional quantum computing. *Frontiers in Physics*, 8, 2020.
- [35] Christopher David White, Chunjun Cao, and Brian Swingle. Conformal field theories are magical. *Physical Review B*, 103(7), 2021.
- [36] Cirq Developers. Cirq, August 2021. See full list of authors on Github: <https://github.com/quantumlib/Cirq/graphs/contributors>.
- [37] Karl Pearson. Note on regression and inheritance in the case of two parents. *Proceedings of the Royal Society of London*, 58:240–242, 1895.
- [38] Daniel A. Roberts and Brian Swingle. Lieb-robinson bound and the butterfly effect in quantum field theories. *Phys. Rev. Lett.*, 117:091602, Aug 2016.
- [39] Ben Craps, Marine De Clerck, Djunes Janssens, Vincent Luyten, and Charles Rabideau. Lyapunov growth in quantum spin chains. *Physical Review B*, 101(17), May 2020.

- [40] O. Bohigas, M. J. Giannoni, and C. Schmit. Characterization of chaotic quantum spectra and universality of level fluctuation laws. *Phys. Rev. Lett.*, 52:1–4, Jan 1984.
- [41] Thomas Guhr, Axel Müller–Groeling, and Hans A. Weidenmüller. Random-matrix theories in quantum physics: common concepts. *Physics Reports*, 299(4–6):189–425, Jun 1998.
- [42] M. V. Berry and M. Tabor. Level clustering in the regular spectrum. *Proceedings of the Royal Society of London. Series A, Mathematical and Physical Sciences*, 356(1686):375–394, 1977.
- [43] Kanato Goto, Tomoki Nosaka, and Masahiro Nozaki. Chaos by magic, 2021.
- [44] Yichen Huang, Fernando G. S. L. Brandão, and Yong-Liang Zhang. Finite-size scaling of out-of-time-ordered correlators at late times. *Phys. Rev. Lett.*, 123:010601, Jul 2019.
- [45] MD SAJID ANIS, Abby-Mitchell, Héctor Abraham, AduOffei, Rochisha Agarwal, Gabriele Agliardi, Merav Aharoni, Ismail Yunus Akhalwaya, and et al. Qiskit: An open-source framework for quantum computing, 2021.
- [46] Lorenzo Leone, Salvatore F. E. Oliviero, and Alioscia Hama. Stabilizer rényi entropy. *Physical Review Letters*, 128(5), feb 2022.
- [47] Tiff Brydges, Andreas Elben, Petar Jurcevic, Benoît Vermersch, Christine Maier, Ben P. Lanyon, Peter Zoller, Rainer Blatt, and Christian F. Roos. Probing rényi entanglement entropy via randomized measurements. *Science*, 364(6437):260–263, apr 2019.
- [48] A. Elben, B. Vermersch, C. F. Roos, and P. Zoller. Statistical correlations between locally randomized measurements: A toolbox for probing entanglement in many-body quantum states. *Physical Review A*, 99(5), may 2019.
- [49] You Zhou, Pei Zeng, and Zhenhuan Liu. Single-copies estimation of entanglement negativity. *Physical Review Letters*, 125(20), nov 2020.
- [50] Salvatore F. E. Oliviero, Lorenzo Leone, Alioscia Hama, and Seth Lloyd. Measuring magic on a quantum processor, 2022.
- [51] Tobias Haug and M. S. Kim. Scalable measures of magic for quantum computers, 2022.
- [52] Arash Ahmadi and Eliska Greplova. Magic Info Scrambling. <https://gitlab.com/QMAI/papers/magicinfoscrumbling>.
- [53] Daniel Gottesman. Fault-tolerant quantum computation with higher-dimensional systems. *Chaos, Solitons & Fractals*, 10(10):1749–1758, Sep 1999.
- [54] Adriano Barenco, Charles H. Bennett, Richard Cleve, David P. DiVincenzo, Norman Margolus, Peter Shor, Tycho Sleator, John A. Smolin, and Harald Weinfurter. Elementary gates for quantum computation. *Physical Review A*, 52(5):3457–3467, nov 1995.
- [55] P. Oscar Boykin, Tal Mor, Matthew Pulver, Vwani Roychowdhury, and Farrokh Vatan. A new universal and fault-tolerant quantum basis. *Information Processing Letters*, 75(3):101–107, 2000.